Naval Research Laboratory
Washington, DC 20375-5000

NRL Memorandum Report 6011

Guiding of Electron Beams by Hollow Conducting Channels

R. F. FERNSLER

Plasma Theory Branch
Plasma Physics Division

B. HUI

Naval Surface Weapons Center
Silver Spring, MD 20903-5000

July 30, 1987

SECURITY CLASSIFICATION OF THIS PAGE

AD-A183683

REPORT DOCUMENTATION PAGE

1a. REPORT SECURITY CLASSIFICATION UNCLASSIFIED	1b. RESTRICTIVE MARKINGS
2a. SECURITY CLASSIFICATION AUTHORITY	3. DISTRIBUTION/AVAILABILITY OF REPORT Approved for public release; distribution unlimited.
2b. DECLASSIFICATION/DOWNGRADING SCHEDULE	
4. PERFORMING ORGANIZATION REPORT NUMBER(S) NRL Memorandum Report 6011	5. MONITORING ORGANIZATION REPORT NUMBER(S)
6a. NAME OF PERFORMING ORGANIZATION Naval Research Laboratory 6b. OFFICE SYMBOL (If applicable) Code 4790	7a. NAME OF MONITORING ORGANIZATION Naval Surface Weapons Center
6c. ADDRESS (City, State, and ZIP Code) Washington, DC 20375-5000	7b. ADDRESS (City, State, and ZIP Code) Silver Spring, MD 20903-5000
8a. NAME OF FUNDING/SPONSORING ORGANIZATION DARPA 8b. OFFICE SYMBOL (If applicable)	9. PROCUREMENT INSTRUMENT IDENTIFICATION NUMBER
8c. ADDRESS (City, State, and ZIP Code) Arlington, VA 22209	10. SOURCE OF FUNDING NUMBERS PROGRAM ELEMENT NO. 62707E PROJECT NO. N60921-86-WR-W0233 TASK NO. ARPA Order #4395, A63 WORK UNIT ACCESSION NO. DN680-415

11. TITLE (Include Security Classification)

Guiding of Electron Beams by Hollow Conducting Channels

12. PERSONAL AUTHOR(S)
Fernsler, R.F. and Hui,* B.

13a. TYPE OF REPORT	13b. TIME COVERED	14. DATE OF REPORT (Year, Month, Day)	15. PAGE COUNT
Interim	FROM _____ TO _____	1987 July 30	50

16. SUPPLEMENTARY NOTATION
*Naval Surface Weapons Center, Silver Spring, MD 20903-5000

17. COSATI CODES		
FIELD	GROUP	SUB-GROUP

18. SUBJECT TERMS (Continue on reverse if necessary and identify by block number)
Relativistic electron beam; Magnetic cage; Channel tracking; Hose instability; Resistive pipe;

19. ABSTRACT (Continue on reverse if necessary and identify by block number)

The use of hollow conducting channels to guide relativistic electron beams through dense gases is explored theoretically. The channel conditions needed to effect strong guidance are determined from analytic and numerical computations of the transverse force felt by a beam uniformly displaced but propagating inside the channel. The force is shown to be strong in the beam head but weak in the beam body. Several different channel configurations are considered, and various effects that can degrade channel guidance are discussed.

Keywords:

20. DISTRIBUTION/AVAILABILITY OF ABSTRACT	21. ABSTRACT SECURITY CLASSIFICATION
☒ UNCLASSIFIED/UNLIMITED ☐ SAME AS RPT. ☐ DTIC USERS	UNCLASSIFIED

22a. NAME OF RESPONSIBLE INDIVIDUAL	22b. TELEPHONE (Include Area Code)	22c. OFFICE SYMBOL
R.F. Fernsler	(202) 767-6786	Code 4790

DD FORM 1473, 84 MAR 83 APR edition may be used until exhausted. All other editions are obsolete.

SECURITY CLASSIFICATION OF THIS PAGE

CONTENTS

GUIDING OF ELECTRON BEAMS BY HOLLOW CONDUCTING CHANNELS

1. Introduction

An electron beam propagating inside a metallic pipe experiences magnetic centering forces caused by return currents induced in the pipe wall. This has led to the suggestion that an annular conducting channel, created by a laser or other means, could guide and possibly stabilize relativistic electron beams propagating through dense gases.[1-3] A potential application is in inertial confinement fusion reactors where multiple beams from isolated diodes propagate through several meters of a dense shielding gas toward a common target.[4] Advantages of hollow-channel guidance over other proposed schemes[4-7] are that it is electrodeless and requires no additional power supplies, it is compatible with the need for a dense shielding gas, it improves beam stability, it can be used repetitively, and the laser light producing the channel can lie outside the target and need not interact with it.

In this paper we provide a theoretical basis for hollow-channel guidance and for the major processes affecting it. The analysis is restricted to gas densities sufficiently high that a scalar conductivity adequately describes the channel electrical properties. To understand the interaction between a beam and hollow channel, we consider a rigid-rod beam that is displaced from the channel axis but propagates inside. The displaced beam experiences a transverse force that is termed "tracking" if the force acts to center the beam in the channel, and is termed "detracking" otherwise. The magnitude and duration of the force are computed analytically and are used to estimate the channel conditions needed for successful guidance. Several channel configurations (thin and

Manuscript approved April 6, 1987

thick annuli, rarefied annuli, and a magnetic cage) are considered. Preliminary computer simulations are presented to support the analysis. All of these tracking schemes are passive in that they rely on channel currents induced by the beam. Not discussed is active magnetic guidance from channel currents that are externally driven. The dynamical response of the beam to the channel forces will be presented in a later paper.

2. Tracking in a Metallic Pipe

To illustrate the nature and magnitude of magnetic tracking, consider a beam propagating inside a perfectly conducting, hollow metallic pipe. Injection of the displaced beam into the pipe induces an image current and charge on the pipe. The pipe return current I_c magnetically repels the beam current I_b, while the distributed pipe charge Q_c electrostatically attracts the distributed beam charge $I_b/\beta c$. Here βc is the axial beam velocity which is taken to be everywhere constant. If the pipe is evacuated and infinitely long with no conducting end plates, $Q_c \to I_c/\beta c$ and the electrostatic forces overcome the magnetic forces to order $\gamma^{-2} = 1 - \beta^2 \ll 1$. The net transverse force on the beam is then weak but detracking and propels the beam into the pipe wall. Self-forces similarly cause the beam to slowly expand.

If the pipe is filled with dense gas, the beam will ionize the gas and generate conductivity σ_b in the immediate vicinity of the beam. This conductivity shorts out the electrostatic fields and forces on the beam, while simultaneously freezing in the magnetic fields and forces. As a result, the beam begins to magnetically pinch and track the pipe center within a charge neutralization time given by

$$\tau_e = 1/4\pi\sigma_b. \qquad (1)$$

Beam ionization causes σ_b to rise rapidly so that the charge-neutralization time for an intense beam in a dense gas is typically subnanosecond. We shall henceforth generally ignore electrostatic effects unless explicitly stated otherwise.

To determine the magnitude of the magnetic tracking force, consider a beam of fixed radius a_b that lies wholly inside a pipe of inner radius $a_c > a_b$. The beam is displaced to an off-axis location $y < a_c - a_b$. In addition to the pipe current I_c, the beam induces a return plasma current I_p in the ionized gas. If the beam and plasma currents are assumed to be azimuthally symmetric about the displaced axis $\underset{\sim}{r}_\perp = \underset{\sim}{y}$, the axial vector potential from these currents is given by

$$A_{z1}(\underset{\sim}{r}_\perp) = \frac{I(|\underset{\sim}{r}_\perp - \underset{\sim}{y}|)}{c} \ln\left(\left|\frac{\underset{\sim}{r}_\perp - \underset{\sim}{y}}{d}\right|^2\right) \qquad (2)$$

where d is a scale length determined by the boundary conditions and $I(|\underset{\sim}{r}_\perp - \underset{\sim}{y}|)$is the net current flowing within a radius $|\underset{\sim}{r}_\perp - \underset{\sim}{y}|$ about the $\underset{\sim}{y}$ axis. Observe that the beam-centered plasma current I_p produces no net tracking force on the beam, although it does alter the magnetic pinch force on the beam. Any asymmetry in the plasma current would, of course, produce additional tracking or detracking forces. We show in Sec. 3 that these forces are often small provided the plasma conductivity σ_b remains centered about the beam. Forces from the plasma currents become important, however, once the beam begins to track (or hose).

Because the beam and plasma currents reside off axis, the induced pipe current I_c is distributed asymmetrically. This asymmetry gives rise to a magnetic centering force on the beam that can be computed by replacing the pipe by an image line-current I_c located at $\underset{\sim}{r}_\perp = \underset{\sim}{y}'$. The image line-current generates an axial vector potential given by[8]

$$A_{z2}(\underset{\sim}{r}_\perp) = \frac{I_c}{c} \ln\left(\left|\frac{\underset{\sim}{r}_\perp - \underset{\sim}{y}'}{d'}\right|^2\right) \tag{3}$$

where d′ is another normalization length. The pipe boundary condition for the total vector potential is

$$A_{z1} + A_{z2} = 0 \tag{4}$$

at $r = a_c$. Combining Eqs. (2)-(4) produces, after some algebraic manipulation, the following results:

$$I_c = - I_n, \tag{5}$$

$$\underset{\sim}{y}' = (a_c/y)^2 \underset{\sim}{y} , \tag{6}$$

and

$$d'/d = a_c/y \tag{7}$$

where $I_n = I_b + I_p$ is the net current. The <u>total</u> current, $I_b + I_p + I_c$, equals zero.

The image line-current I_c located at $\underset{\sim}{y}'$ repels the beam current I_b located at $\underset{\sim}{y}$ with a distributed force given by

$$N_b \underset{\sim}{F}_m = \frac{2}{c^2} \frac{I_b I_c}{|\underset{\sim}{y}' - \underset{\sim}{y}|^2} (\underset{\sim}{y}' - \underset{\sim}{y}) = - \frac{2}{c^2} \frac{I_b I_n}{a_c^2 - y^2} \underset{\sim}{y}. \tag{8}$$

The average magnetic tracking force per beam electron is thus

$$\underset{\sim}{F}_m = \frac{2e\beta}{c} \frac{I_n}{a_c^2 - y^2} \underset{\sim}{y} \tag{9}$$

where $N_b = -I_b/e\beta c$ is the beam line density. Result (9) characterizes the maximum magnetic tracking force that a hollow conducting channel can exert on a beam. Note that F_m attains a magnitude comparable to the average monopole pinch force, $F_o = e\beta I_n/a_b c$, as the displacement $y \to a_c - a_b$.

Although the transverse beam force is tracking, the transverse force on the counter-flowing plasma current I_p is detracking. In a dense gas the plasma channel does not physically displace, but the plasma electrons instead establish a Hall electrostatic field to offset the magnetic detracking force:

$$\underset{\sim}{E}_H = \frac{2v_d}{c^2} \frac{I_n}{a_c^2 - y^2} \underset{\sim}{y} \tag{10}$$

where v_d is the axial plasma-electron drift velocity. This Hall field produces a weak detracking force on the beam electrons which can be ignored to order

$$eE_H/F_m = v_d/\beta c << 1. \tag{11}$$

The force would be tracking if the beam and plasma current-carriers were oppositely charged. The Hall effect also produces a slight lateral shift in the plasma current that has a yet weaker influence on tracking.

3. Tracking in a Conducting Gaseous Annulus

Replacing the metallic pipe with a preionized and conducting gaseous annulus introduces three new features. Two arise from the finite conductance of the annulus. The third arises from the tenuousness of the annulus which permits beam electrons to easily penetrate it.

The first new feature is that electrostatic fields between the inner and ou er radii of the annulus are no longer fully suppressed. These fields reduce the return current carried by the annulus and thereby reduce the magnetic tracking force on the beam. Although the channel charge and corresponding electrostatic detracking force are similarly reduced, an additional detracking force arises from bipolar charging of the channel. Positive and negative charge sheaths form on the inner and outer channel edges, respectively, to produce an electrostatic detracking force that is the analogue of the tracking force produced by solid channels.[9] A very low conductivity in a hollow channel thus produces a net beam force that is initially detracking although weak.

The second new feature is that magnetic flux diffuses through the resistive annulus. Any azimuthal asymmetry in the channel current thus relaxes on a finite channel dipole decay time τ_{c1}. Because a symmetric channel current produces no fields or forces on beam electrons inside the channel, the channel tracking force relaxes on τ_{c1}. The integrated channel current I_c relaxes on a channel monopole time τ_{co} which is usually longer, $\tau_{co} > \tau_{c1}$.

Spreading of the beam through the gaseous channel is the third new feature. A circular ring of beam current which lies entirely outside the channel produces zero electromagnetic field inside the ring, due to the assumed azimuthal symmetry of the beam. Such a ring thus experiences zero net force from the channel. A ring which passes through the channel always experiences, however, a detracking force caused by channel return current flowing outside the ring; see Fig. 1. The net magnetic force on a beam with an extended radial profile is thus comprised of a tracking component from beam rings inside the channel, and a detracking component from beam

rings intersecting the channel. At late times only the detracking component survives. The detracking effect from the beam wings was ignored in deriving Eq. (9).

These new features suggest that a conducting annular channel can strongly guide an electron beam only if three conditions are met. First, the channel should have sufficient conductivity σ_c to suppress internal electrostatic fields: typically,

$$4\pi\sigma_c a_c/c \gtrsim 1 \tag{12}$$

where a_c is the inner channel radius. Otherwise, electrostatic detracking of the beam head may take place.

Second, the magnetic tracking force from the channel current should persist longer than the electrostatic detracking force from the channel charge. Strong magnetic tracking can thus occur only if the channel magnetic dipole decay time exceeds the beam charge-neutralization time,

$$\tau_{c1} > \tau_e. \tag{13}$$

At the beam pinch point where[10]

$$4\pi\sigma_b a_{bp}/c = 1, \tag{14}$$

condition (13) reduces with the help of definition (1) to

$$\tau_{c1} > a_{bp}/c. \tag{15}$$

Here a_{bp} is the beam radius at the pinch point.

The third condition is that the annulus should lie outside the beam to minimize magnetic detracking by the beam wings:

$$a_c > a_{bp} + y. \tag{16}$$

If the latter condition is not met, the hollow channel can act as a solid channel and eject the beam via magnetic repulsion from the opposing channel current. Increasing the inner channel radius to much beyond requirement (16) decreases, however, the tracking force as Eq. (9) demonstrates. Optimal beam guidance is therefore expected to occur when

$$1 < a_c/a_{bp} < 2. \tag{17}$$

When conditions (12), (15) and (16) are satisfied, the net force on the beam head is tracking and remains tracking (in dense gases) to beyond the pinch point. After the pinch point, magnetic coupling forces become strong and can overcome any residual detracking force arising from beam-channel overlap. The coupling forces thus cause the beam body to follow the head. These same coupling forces also give rise to the resistive hose instability[11,12] briefly discussed in Sec. 3.4.

3.1 Linearized Analysis

Investigating the consequences of condition (15) requires computation of the channel dipole decay time τ_{c1}. To compute this time and to analyze the problem in further detail, we use Ampere's law for the axial vector potential A_z:

$$\nabla_\perp^2 A_z = - \frac{4\pi}{c} \left(J_b - \sigma \frac{\partial A_z}{\partial \zeta} \right) \tag{18}$$

where J_b is the beam current density, σ is the plasma conductivity, and $\zeta \equiv ct-z$ is the distance behind the beam head. Here we have employed both the ultrarelativistic frozen approximation,

$$\left(\frac{\partial}{\partial z}\right)_\zeta = 0, \tag{19}$$

and the magnetostatic approximation,

$$E_z = -\frac{\partial}{\partial \zeta}(A_z - \phi) \simeq -\frac{\partial A_z}{\partial \zeta} \tag{20}$$

where E_z is the axial electric field and ϕ is the electrostatic potential. The neglect of ϕ is strictly justified only within the annulus itself, where $4\pi\sigma_c a_c/c > 1$, and behind the pinch point, where $4\pi\sigma_b a_b/c > 1$. Ahead of the pinch point, our results for the magnitude and duration of the magnetic channel tracking force still apply, at least approximately, when expressed in terms of the channel current I_c; in this region, however, I_c depends strongly on ϕ. Not computed in this analysis are electrostatic effects (such as detracking by channel charge) which are complicated by the dynamics of space-charge neutralization.

To simplify the problem, we consider small displacements $y \ll a_b < a_c$ and divide the plasma conductivity into two components. The component σ_b is azimuthally symmetric about the beam axis $\underset{\sim}{r}_\perp = \underset{\sim}{y}$, while the component σ_c is azimuthally symmetric about the channel axis $\underset{\sim}{r}_\perp = 0$. As discussed in Secs. 4 and 5, processes such as avalanching and high-order chemistry effects can complicate and modify this separation of σ. Here we ignore these complications and perform a straightforward linearized azimuthal expansion about the channel axis:

$$A_z(r,\theta,\zeta) = A_o(r,\zeta) + A_1(r,\zeta)\cos\theta + \ldots \tag{21a}$$

$$J_b(r,\theta,\zeta) = J_b(r',\zeta) - y\frac{\partial J_b}{\partial r'}\cos\theta + \ldots \tag{21b}$$

$$\sigma_b(r,\theta,\zeta) = \sigma_b(r',\zeta) - y\,\frac{\partial \sigma_b}{\partial r'}\cos\theta + \ldots \qquad (21c)$$

where $r' = |\underset{\sim}{r}_\perp - \underset{\sim}{y}|$. We treat the dipole terms as small perturbations and set $r' = r$. Inserting expansion (21) into Eq. (18) then yields

$$\frac{1}{r}\frac{\partial}{\partial r}\, r\,\frac{\partial A_o}{\partial r} = -\frac{4\pi}{c}\left[J_b - (\sigma_b + \sigma_c)\,\frac{\partial A_o}{\partial \zeta}\right] \qquad (22)$$

for the monopole potential A_o, and

$$\frac{\partial}{\partial r}\,\frac{1}{r}\,\frac{\partial}{\partial r}\, rA_1 = \frac{4\pi}{c}\left[y\,\frac{\partial J_b}{\partial r} - y\,\frac{\partial \sigma_b}{\partial r}\,\frac{\partial A_o}{\partial \zeta} + (\sigma_b + \sigma_c)\,\frac{\partial A_1}{\partial \zeta}\right] \qquad (23)$$

for the dipole potential A_1.

Each beam electron experiences a transverse magnetic force given by

$$\underset{\sim}{F}_{me} = -e\beta\,\underset{\sim}{\nabla}_\perp A_z. \qquad (24)$$

The average tracking force for the entire beam is thus

$$F_m = -e\beta\iint d^2 r_\perp\,\frac{J_b}{I_b}\,\hat{y}\cdot\underset{\sim}{\nabla}_\perp A_z$$

$$= -e\beta\int_o^\infty dr\; r\int_o^{2\pi} d\theta\,\frac{J_b}{I_b}\left(\cos\theta\,\frac{\partial A_z}{\partial r} - \frac{\sin\theta}{r}\,\frac{\partial A_z}{\partial \theta}\right) \qquad (25)$$

where $\hat{y}$ is the unit displacement vector. Substituting expansion (21) into Eq. (25) produces

$$F_m = -\frac{e\beta\pi}{I_b}\int_o^\infty dr\; r\left[J_b\left(\frac{1}{r}\,\frac{\partial}{\partial r}\, rA_1\right) - y\,\frac{\partial J_b}{\partial r}\,\frac{\partial A_o}{\partial r}\right]. \qquad (26)$$

Integrating both terms by parts and using the dipole boundary condition,

$$\lim_{r\to\infty} \left(\frac{1}{r}\frac{\partial}{\partial r} rA_1\right) = 0, \tag{27}$$

we obtain

$$F_m = \frac{e\beta}{2}\int_0^\infty dr\left[\hat{I}_b\left(\frac{\partial}{\partial r}\frac{1}{r}\frac{\partial}{\partial r} rA_1\right) - y\frac{\partial\hat{I}_b}{\partial r}\left(\frac{1}{r}\frac{\partial}{\partial r} r\frac{\partial A_o}{\partial r}\right)\right]. \tag{28}$$

Here the beam radial profile is defined by

$$\hat{I}_b(r,\zeta) = \int_0^r dr\, 2\pi r\, J_b(r,\zeta)/I_b(\zeta). \tag{29}$$

Substituting expressions (22) and (23) into Eq. (28) produces

$$F_m = \frac{2\pi e\beta}{c}\int_0^\infty dr\left\{\hat{I}_b\left[y\frac{\partial J_b}{\partial r} - y\frac{\partial\sigma_b}{\partial r}\frac{\partial A_o}{\partial\zeta} + \left(\sigma_b + \sigma_c\right)\frac{\partial A_1}{\partial\zeta}\right]\right.$$

$$\left. + y\frac{\partial\hat{I}_b}{\partial r}\left[J_b - \left(\sigma_b + \sigma_c\right)\frac{\partial A_o}{\partial\zeta}\right]\right\} \tag{30}$$

Integrating the first two terms by parts reduces this to

$$F_m = \frac{2\pi e\beta}{c}\int_0^\infty dr\left[\hat{I}_b\sigma_c\frac{\partial A_1}{\partial\zeta} - y\frac{\partial\hat{I}_b}{\partial r}\sigma_c\frac{\partial A_o}{\partial\zeta} + \hat{I}_b\sigma_b\frac{\partial A_{1b}}{\partial\zeta}\right] \tag{31}$$

where

$$A_{1b} \equiv A_1 + y\frac{\partial A_o}{\partial r}. \tag{32}$$

Result (31) for the average magnetic deflection force F_m has the following physical basis. The first term in the integrand, $\hat{I}_b\ \sigma_c\ \partial A_1/\partial\zeta$, represents the contribution from channel dipole currents that produce the channel tracking force previously described. The second term, $-y\ \partial\hat{I}_b/\partial r\ \sigma_c\ \partial A_o/\partial\zeta$, represents the channel detracking force caused by overlap of the beam current ($J_b \propto \partial\hat{I}_b/\partial r$) and the channel current ($J_c = -\sigma_c\ \partial A_o/\partial\zeta$). The last term, $\hat{I}_b\ \sigma_b\ \partial A_{1b}/\partial\zeta$, arises from plasma current in the beam-centered conductivity σ_b. This plasma current produces a net transverse force on the beam only if it is asymmetrically distributed with respect to the beam. Here A_{1b} is the dipole potential for an expansion about the beam axis $\underset{\sim}{r}_\perp = \underset{\sim}{y}$. This potential is defined by Eq. (32) and satisfies

$$\frac{\partial}{\partial r}\frac{1}{r}\frac{\partial}{\partial r}\,rA_{1b} = \frac{4\pi}{c}\left[y\,\frac{\partial\sigma_c}{\partial r}\,\frac{\partial A_o}{\partial\zeta} + (\sigma_b + \sigma_c)\,\frac{\partial A_{1b}}{\partial\zeta}\right]. \tag{33}$$

3.2 Thin Annulus ("Resistive Pipe")

The magnitude and duration of the tracking and detracking components of F_m can be computed using Eqs. (22), (23), and (33). To further simplify the problem, consider first a narrow channel with a specified distributed resistance $R_c(\zeta)$:

$$\sigma_c(r,\zeta) = \delta(r - a_c)/2\pi a_c R_c(\zeta) \tag{34}$$

where δ is the Dirac delta function. Inserting this form into Eq. (23), applying boundary condition (27) and definition (32), and performing two radial integrations yields for the channel dipole potential

$$A_1(a_c,\zeta) = -\int_0^{a_c} dr\, r \int_r^{\infty} dr\, \frac{4\pi}{a_c c}\left[\sigma_c \frac{\partial A_1}{\partial \zeta} + y \frac{\partial}{\partial r}\left(J_b - \sigma_b \frac{\partial A_o}{\partial \zeta}\right)\right.$$

$$\left. + \sigma_b \frac{\partial}{\partial \zeta}\left(A_1 + y \frac{\partial A_o}{\partial r}\right)\right]$$

$$= -\frac{1}{R_c c}\frac{\partial}{\partial \zeta} A_1(a_c,\zeta) + \frac{y}{a_c}\frac{2I(a_c,\zeta)}{c}$$

$$- \frac{4\pi}{a_c c}\int_0^{a_c} dr\, r \int_r^{\infty} dr\, \sigma_b \frac{\partial}{\partial \zeta} A_{1b}. \qquad (35)$$

Here the net current flowing just inside the channel is given by

$$I(a_c,\zeta) = \int_0^{a_c} dr\, 2\pi r\left(J_b - \sigma_b \frac{\partial}{\partial \zeta} A_o\right). \qquad (36)$$

Inspection of the term on the left and the first term on the right of Eq. (35) indicates that $A_1(a_c,\zeta)$ relaxes on a characteristic dipole decay length given by

$$c\tau_{c1} = 1/R_c c. \qquad (37)$$

The channel dipole current and tracking force relax similarly.

Applying the same technique to Eq. (22) yields for the channel monopole potential

$$A_o(a_c,\zeta) = -\frac{2\ \ln(b/a_c)}{R_c c}\frac{\partial}{\partial \zeta} A_o(a_c,\zeta) + \frac{2}{c}\int_{a_c}^{b}\frac{dr}{r} I(r,\zeta) \qquad (38)$$

where $b > a_c$ is the monopole boundary radius and $I(r,\zeta)$ is the net current, exclusive of the channel current, flowing within radius r:

$$I(r,\zeta) \equiv \int_0^r dr\ 2\pi r\left(J_b - \sigma_b \frac{\partial A_o}{\partial \zeta}\right). \tag{39}$$

Inspection of Eq. (38) indicates that the channel monopole potential, field, and current relax on a characteristic monopole decay length given by

$$c\tau_{co} = (2/R_c c)\ln(b/a_c). \tag{40}$$

The channel monopole and dipole decay times are thus related by

$$\tau_{co}/\tau_{c1} = 2\ \ln(b/a_c). \tag{41}$$

The boundary radius b in these equations is where the monopole electric field falls to zero:

$$E_{zo}(b,\zeta) = 0. \tag{42a}$$

In the magnetostatic limit considered here, we impose the equivalent condition that

$$A_o = 0 \tag{42b}$$

for all $r \geq b$. In the absence of external return-current structures, as was assumed for the dipole boundary condition (28), the monopole boundary radius b equals the vacuum radius b_{vac} where the conductivity becomes too low to neutralize the space-charge fields. Typically,

$$4\pi\sigma r/c \lesssim 0.1 \tag{43}$$

for all $r \geq b_{vac} > a_c$. If a metallic pipe or similar structure is present at a radius b_{pipe}, the boundary b equals the lesser of b_{pipe} and b_{vac}. More importantly, the dipole boundary condition (28) must then be replaced

with the requirement that $A_1(b_{pipe},\zeta) = 0$. This requirement gives rise to an additional magnetic tracking force caused by return currents induced in the pipe.

We have thus far shown that the channel tracking force, as represented by the first term in the integrand of Eq. (31), relaxes on a channel dipole time $\tau_{c1} = 1/R_c c^2$. The second term, which represents a detracking force from beam-channel overlap, relaxes more slowly on a channel monopole time $\tau_{co} > \tau_{c1}$. The detracking force is small, however, if the overlap is small. From Eqs. (31), (35) and (38) one can show that the ratio of the overlap detracking force to the tracking force is initially given by

$$|F_{co}/F_t| = \pi a_c^2 J_b(a_c,\zeta)/I_b(a_c,\zeta) \leq 1 \qquad (44)$$

where $I_b(a_c,\zeta)$ is the beam current within $r = a_c$. This result can also be inferred by using Fig. 1 to estimate the detracking force from beam-channel overlap and comparing it to the tracking force given by Eq. (9). For the infinitesimally thin channels considered here, the net channel tracking force is maximized for Bennett or flat-topped beams when $a_c = a_b$. For channels of finite breadth, maximum tracking is generally realized when condition (17) is satisfied. If $a_c > 2a_{bp} + y$, the detracking force can usually be neglected altogether.

We have yet to assess the last term in Eq. (31) which represents the dipole force arising from plasma current induced in the beam-generated conductivity σ_b. This component of the tracking force was neglected in the nonlinear derivation given in Sec. 2. We show here that such neglect is often well justified, provided the beam is rigidly displaced. This component becomes important, however, once the beam begins to track or hose.

is the beam-centered resistance per unit length. Equations (46) and (47b) indicate that A_{1b} relaxes on a characteristic dipole decay length given by

$$c\tau_{b1} \simeq 1/R_b c = \pi a_b^2 \sigma_b / c. \tag{49}$$

The detracking force from dipole currents in the beam-centered conductivity σ_b [i.e., the last term in Eq. (32)] thus relaxes on a time $\tau_{b1} \simeq (R_c/R_b)\tau_{c1}$. This detracking is short-lived and can be neglected if $R_b >> R_c$, as is usually true in the beam head.

In evaluating the characteristic relaxation times for A_{1b} and $A_1(a_c,\zeta)$, we neglected the coupling between them. Such coupling alters the actual relaxation times and thereby alters the tracking force. The maximum effect that A_{1b} has on $A_1(a_c,\zeta)$ can be estimated by using Eqs. (46) and (47b) to compute an approximate upper bound for $\partial/\partial\zeta\, A_{1b}$:

$$\left(\frac{\partial A_{1b}}{\partial \zeta}\right)_{max} \simeq - \frac{(r/a_c)}{1-r^2/2a_b^2} \left(\frac{R_b}{R_c}\right) \frac{\partial A_1(a_c,\zeta)}{\partial \zeta}. \tag{50}$$

Substituting this upper bound into Eq. (35) produces

$$A_1(a_c\zeta) = - \frac{1}{R_c c} \frac{\partial}{\partial \zeta} A_1(a_c,\zeta) + \frac{y}{a_c} \frac{2I(a_c,\zeta)}{c}$$

$$+ \frac{4\pi}{a_c^2 c} \left(\frac{R_b}{R_c}\right) \frac{\partial}{\partial \zeta} A_1(a_c,\zeta) \int_0^{a_b} dr\, r \int_r^{a_b} dr\, \sigma_b \frac{r}{1-r^2/2a_b^2} \tag{51}$$

where the limits in the integrands have been changed to reflect the assumption that $\sigma_b \to 0$ for $r > a_b$. For flat σ_b, we can readily evaluate the integrals and rewrite Eq. (51) as

$$\left[1 - \alpha \frac{a_b^2}{a_c^2}\right] \frac{1}{R_c c} \frac{\partial A_1(a_c,\zeta)}{\partial \zeta} = \frac{y}{a_c} \frac{2I(a_c,\zeta)}{c} - A_1(a_c,\zeta) \tag{52}$$

where $\alpha = \ln(16) - 2 \approx 0.77$. In this example, $A_1(a_c,\zeta)$ thus relaxes on a time τ_{c1}' that is somewhat shorter than $\tau_{c1} = 1/R_c c^2$:

$$\tau_{c1}'/\tau_{c1} = 1 - \alpha\,(a_b/a_c)^2 > 0.23. \qquad (53)$$

For $a_c \geq 1.5\, a_b$, $\tau_{c1}' > \tau_{c1}/2$. Moreover, if $R_b >> R_c$ as is usually true in the beam head, $\tau_{c1}' \to \tau_{c1}$ regardless of the ratio a_c/a_b.

The accelerated relaxation of $A_1(a_c,\zeta)$ increases the maximum channel tracking force while decreasing its duration. The increase in magnitude represents the reactive response of the conducting channel to the detracking current induced in σ_b. The net tracking force is nonetheless weakened. In the absence of beam-channel overlap, the maximum net tracking force is given from Eqs. (31), (50), and (52) by

$$F_m^{(max)} = \left[\frac{0.23}{1-0.77a_b^2/a_c^2}\right] \frac{2e\beta y I(a_c,\zeta)}{a_c^2 c}. \qquad (54)$$

Here we have assumed flat J_b (i.e., $\hat{I}_b = r^2/a_b^2$) for $r \leq a_b$. Except for the term in square brackets, Eq. (54) represents the linearized equivalent of Eq. (9) in the limit $y << a_c$. The term in brackets represents the maximum reduction in the tracking force from dipole currents in σ_b. If $R_b >> R_c$, no reduction occurs, and the term in brackets should be set to unity.

3.3 Thick Annulus

Consider now the opposite limit of a broad, hollow conducting annulus for which $\sigma_c = 0$ for $r < a_c$. If we neglect both beam-channel overlap ($a_b < a_c$) and all effects from dipole currents in σ_b, Eqs. (23) and (31) reduce respectively to

$$\frac{\partial}{\partial r}\frac{1}{r}\frac{\partial}{\partial r} rA_1 \simeq \frac{4\pi}{c}\left[y\frac{\partial}{\partial r}\left(J_b - \sigma_b\frac{\partial A_o}{\partial \zeta}\right) + \sigma_c\frac{\partial A_1}{\partial \zeta}\right] \tag{55}$$

and

$$F_m \simeq \frac{2\pi e\beta}{c}\int_{a_c}^{\infty} dr\ \sigma_c\frac{\partial A_1}{\partial \zeta}. \tag{56}$$

Here we have used definition (32) to rewrite and eliminate all terms containing $\sigma_b\ \partial A_{1b}/\partial\zeta$ from Eq. (23), and have set $\dot{I}_b = 1$ for $r \geq a_c$ in Eq. (31).

By integrating Eq. (55) twice, we obtain with the help of Eqs. (27) and (39) for all $r \leq a_c$,

$$rA_1 = -\frac{4\pi}{c}\int_o^r dr\ r\int_r^{\infty} dr\left[y\frac{\partial}{\partial r}\left(J_b - \sigma_b\frac{\partial A_o}{\partial \zeta}\right) + \sigma_c\frac{\partial A_1}{\partial \zeta}\right]$$

$$= \frac{2y}{c}I(r,\zeta) - \frac{2\pi r^2}{c}\int_{a_c}^{\infty} dr\ \sigma_c\frac{\partial A_1}{\partial \zeta} \tag{57}$$

where we have used the fact that $\sigma_c = 0$ for $r < a_c$. Combining this with Eq. (56) yields

$$F_m(\zeta) = \frac{2e\beta y I(r,\zeta)}{r^2 c} - \frac{e\beta A_1(r,\zeta)}{r} \tag{58}$$

for all $r \leq a_c$. This equation demonstrates that diffusion of the internal dipole potential A_1 controls the evolution of the channel tracking force. At late times, $A_1 \to 2yI(r,\zeta)/rc$ while $F_m \to 0$.

To estimate the characteristic relaxation rate for F_m, we take σ_c to be flat and constant:

$$\sigma_c(r) = \sigma_{co}\, H(r-a_c) \tag{59}$$

where H is the Heaviside step function. The solution to Eq. (55) for $r \geq a_c$ and for constant or slowly varying $I(a_c,\zeta)$ is then given by

$$A_1(r,\zeta) = \frac{2yI(a_c,\zeta)}{rc}\, e^{-\pi\sigma_{co}r^2/c\zeta}. \tag{60}$$

Because A_1 must be everywhere continuous, Eqs. (58) and (60) may be combined at $r = a_c$ to produce

$$F_m(\zeta) = \frac{2e\beta yI(a_c,\zeta)}{a_c^2 c}\left(1-e^{-\pi\sigma_{co}a_c^2/c\zeta}\right). \tag{61}$$

The characteristic relaxation length for the tracking force produced by a broad hollow channel of inner radius a_c and conductivity σ_{co} is thus

$$c\tau_{c1} = \pi a_c^2 \sigma_{co}/c. \tag{62}$$

Note that the tracking force in broad channels does not follow the simple exponential decay $[\exp(-\zeta/c\tau_{c1})]$ predicted for narrow channels. The slow decay in broad channels occurs because the dipole channel tracking current diffuses radially outward before it decays. The diffusion is reflected in Eqs. (60) and (61).

3.4 Optimal Channel Parameters

We now restate the channel parameters needed to effect strong magnetic tracking at the beam pinch point. We consider both broad and narrow conducting annuli and arbitrarily assume that the beam radius at the pinch point, as defined by condition (14), is $a_{bp} = 3$ cm. This is the main beam parameter that influences the choice of optimal channel parameters.

The optimal inner channel radius is given by condition (17), which is a compromise between channel tracking and the detracking caused by beam-channel overlap. A reasonable choice is $a_c = 5$ cm for $a_{bp} = 3$ cm.

The minimum channel conductivity needed to subdue internal channel electrostatics is given by condition (12): $\sigma_{co} \gtrsim c/4\pi a_c \simeq 5 \times 10^8\ s^{-1}$ for $a_c = 5$ cm. This typically corresponds to a channel ionization fraction of $n_{ec}/n_g \gtrsim 2 \times 10^{-7}$ where n_{ec} is the channel electron density and n_g is the gas density. The gas is thus weakly ionized. The low degree of ionization suggests that the channel could be created using a laser to ionize a seed gas added to an inert base gas.[2]

For thin annuli of width $\delta a_c \ll a_c$, the magnetic conditions (15) and (37) impose an upper bound on the channel resistance:

$$R_c < 1/a_{bp}\, c. \tag{63}$$

This condition insures that magnetic tracking outlasts and dominates electrostatic detracking. For $a_{bp} = 3$ cm, a channel resistance of $R_c < 10^{-11}\ s/cm^2 = 10\ \Omega/cm$ is sufficient. To obtain low R_c for $\delta a_c \ll a_c$ requires, however, a channel conductivity much higher than stipulated by condition (12):

$$4\pi\sigma_{co}a_c/c = 2/R_c\delta a_c c > 2a_{bp}/\delta a_c >> 1. \qquad (64)$$

Such high conductivity is difficult to establish and maintain in dense gases. Narrow conducting hollow channels are thus often impractical for tracking (particularly if formed by lasers or similar gas-ionization methods).

For broad channels of width $\delta a_c \gtrsim a_c$, condition (64) is replaced by

$$4\pi\sigma_{co}\, a_c/c > 4\, a_{bp}/a_c \qquad (65)$$

which is derived using Eqs. (15) and (62). In the present example, condition (65) is only slightly more stringent than condition (12) and is satisfied for $\sigma_{co} > 10^9\ s^{-1}$. The total channel resistance still satisfies condition (63). Note that channel conductivity generated outside $r = 2a_c$ is of little benefit to tracking (although it can aid beam stability).

Satisfying the magnetic condition (15) provides two additional benefits. One is that the channel dipole decay time τ_{c1} is larger than four times the beam dipole decay time τ_{b1} at the pinch point ζ_p:

$$\tau_{c1} > a_{bp}/c = 4\tau_{b1}(\zeta_p). \qquad (66)$$

Magnetic detracking from dipole currents in σ_b can therefore be safely neglected up to and somewhat beyond the pinch point.

A second and potentially more important benefit is the impact that condition (66) has on beam stability. The most virulent instability is beam hose which develops when a nonrigid beam displacement gets out of phase with the induced restoring forces. The phase delay and growth rate for this instability are governed by the dipole decay time.[11] A hollow conducting channel increases the dipole decay time and thus imposes an upper bound on the hose growth rate. In the beam head where $\tau_{c1} >> \tau_{b1}$,

hose develops as a resistive wall instability with a growth rate proportional to τ_{c1}^{-1}. In the beam body where σ_b becomes large and $\tau_{b1} >> \tau_{c1}$, the usual resistive hose instability[11,12] develops with a growth rate proportional to τ_{b1}^{-1}. A hollow channel can thus reduce hose growth in the beam head, and thereby indirectly reduce hose growth (but not the growth rate) in the beam body. A hollow channel additionally lessens hose instability (and axisymmetric instabilities) by reducing the destabilizing plasma return current in the immediate vicinity of the beam.[1] Although the present analysis is restricted to rigid beams, we note that the stabilizing influence of hollow channels has been observed both numerically[1,13] and experimentally.[2,14]

4. Alternative Schemes

A variation on the resistive pipe is a magnetic cage[14] consisting of a ring of three or more solid conducting channels encircling the beam. A four-conductor cage is depicted in Fig. 2. The azimuthal asymmetry of the cage strengthens the tracking force along some directions but weakens it along others. At late times when the channel current has become equally distributed, the force becomes detracking for beam deflections between adjacent channels, even in the absence of beam-channel overlap. The beam head nonetheless tracks and guides the beam body. The cage is thus an acceptable alternative to smooth annular channels, although it does slightly degrade tracking and requires a higher degree of local gas ionization to obtain a given net resistance R_c. The ability of a cage to guide and stabilize a beam was demonstrated experimentally by Raleigh and Fernsler[14] using four resistive rods.

Creating high channel ionization for either the pipe or cage mode can be a formidable problem. One means of circumventing this problem is to utilize avalanching in the space-charge fields of the beam.[2] The space-charge fields peak off axis and are capable of creating high conductivity outside an intense beam. If a rarefied or weakly preionized hollow channel surrounds the beam, preferential avalanching can transform the channel into a good conductor.

The degree of rarefaction or preionization required to create a conducting channel suitable for tracking can be estimated as follows. Avalanching causes the conductivity outside the beam to grow according to

$$c \frac{\partial}{\partial \zeta} \sigma = \rho \tilde{\nu} \sigma \tag{67}$$

where ρ is the local gas density and $\tilde{\nu}(E/\rho)$ is the reduced avalanche rate. Here we have dropped the convective terms (as is often done in simulations) because they little affect the final conductivity. Also dropped is beam direct-production on the assumption that $J_b \to 0$ for $r \geq a_c > a_b$.

In the low-conductivity regions ($4\pi\sigma r/c \ll 1$) outside the beam, the dominant electric field is the radial field E_r which in axisymmetry evolves as

$$\frac{\partial}{\partial \zeta} E_r + \frac{4\pi\sigma}{c} E_r = \frac{\partial}{\partial \zeta} B_\theta. \tag{68}$$

If avalanching is to be effective, the azimuthal magnetic field B_θ changes little during the breakdown process. Dropping the right-hand side of Eq. (68) and setting the total electric field $E \simeq E_r$ allows us to combine and integrate Eqs. (67) and (68) to obtain

$$4\pi\sigma(r,\zeta) \simeq 4\pi\sigma_i(r) + \rho \int_{E}^{E_o} \frac{dE}{E} \tilde{\nu}(E/\rho). \tag{69}$$

Here $\sigma_i(r) = \sigma(r,0)$ is the preexisting conductivity, $E(r,\zeta)$ is the instantaneous electric field, and $E_o(r,\zeta)$ is the effective initial field given by

$$E_o(r,\zeta) = B_\theta(r,\zeta) \simeq 2I(r,\zeta)/rc. \tag{70}$$

Because B_θ is not truly constant, Eqs. (69) and (70) actually represent only an approximate upper bound for the conductivity σ outside the beam. The equations are fairly accurate, however, in the region of greatest interest where $4\pi\sigma r/c \simeq 1$.

If the initial preionization is small, the final conductivity after breakdown is given by

$$4\pi\sigma_f \simeq \rho \int_{E_b}^{E_o} \frac{dE}{E} \tilde{\nu}(E/\rho) >> 4\pi\sigma_i \tag{71}$$

where the breakdown field strength in air is $E_b/\rho \simeq 30$ kV/cm-atm. That σ_f is largely independent of σ_i indicates that preionization alone is unlikely to produce a well-defined hollow conducting channel suitable for tracking.

Potentially more effective is a low-density channel for which the product ρr is small within the channel but large everywhere outside the channel and beam. If $\tilde{\nu}$ is a strong function of E/ρ, as usually true, σ_f is large only within the channel. According to Eq. (71), the channel conductivity produced by avalanching is then limited to

$$4\pi\sigma_c \leq 4\pi\sigma_f(a_c,\zeta) < \rho_c\,\tilde{\nu}(\hat{E}_o/\rho_c) \tag{72}$$

where ρ_c is the channel density and

$$\hat{E}_o \equiv E_o(a_c,\zeta) \simeq 2I(a_c,\zeta)/a_c c. \tag{73}$$

To obtain high conductivity satisfying condition (12) over a broad channel thus typically requires

$$\rho_c\,\tilde{\nu}(\hat{E}_o/\rho_c) >> c/a_c. \tag{74}$$

Condition (74) together with Eq. (73) defines an allowed range for the channel density ρ_c in terms of the avalanche function $\tilde{\nu}$, the inner channel radius a_c, and the net current $I(a_c,\zeta)$ evaluated at the pinch point ζ_p. The maximum channel density allowed by condition (74) depends sensitively on the pinch-point current $I(a_c,\zeta_p)$ which evolves slowly as the beam head erodes. The ambient gas density at $r < a_c$ should satisfy

$$\rho_o \gtrsim 2\,\rho_c \tag{75}$$

to produce a well-defined channel.

The use of avalanching to produce hollow conducting channels has a second important advantage that is not readily apparent from the preceding axisymmetric analysis. A displaced beam introduces azimuthal asymmetry into the channel space-charge fields. This asymmetry is amplified by the avalanche function $\tilde{\nu}(E/\rho)$ to produce a channel conductivity σ_c peaked nearest the beam. The asymmetry in σ_c enhances the asymmetry in the channel return current and thus enhances the channel tracking force. The nonlinear character of $\tilde{\nu}$ can produce a strong asymmetry in σ_c that could raise the tracking force by more than a factor of two. At late times, the

force remains tracking. Even channels that are weakly preionized but not rarefied may be capable of producing modest tracking forces via asymmetric avalanching. Asymmetric avalanching is likely, however, to degrade beam stability.

Although channel rarefaction can produce strong tracking, it is not an energy-efficient process. The hydrodynamic energy required to halve the ambient gas density is orders of magnitude higher than the ionization energy required to create the necessary channel conductivity directly. Tracking experiments in rarefied channels of modest length may nonetheless be practical if direct gas ionization techniques are not readily available.[15]

5. Other Effects

We describe here several other effects that can influence tracking. The first is beam rise time. If the beam current rises slowly, it generates conductivity σ_b gradually so that the pinch point, as defined by condition (14), occurs late in the beam pulse. If the pinch point occurs at a location $\zeta_p >> c\tau_{c1}$, the tracking force is reduced by the fraction $(c\tau_{c1}/\zeta_p) << 1$, as suggested by Eqs. (61) and (62). To minimize this reduction, the channel dipole decay time should therefore satisfy

$$c\tau_{c1} > \zeta_p. \tag{76a}$$

This imposes an additional constraint on either or both the channel resistance R_c and conductivity σ_{co}, as required by either result (37) or (62). For a pencil beam with a constant rise rate $\dot{I}_b$, the pinch point occurs at $\zeta_p \leq c\,(a_b/2k\dot{I}_b)^{1/2}$. Condition (76a) is thus typically satisfied provided

$$\tau_{c1} > (a_{bp}/2k\dot{I}_b)^{1/2}. \tag{76b}$$

Here a_{bp} is the beam radius at the pinch point, and k is the direct-production coefficient defined through the relationship

$$\frac{\partial \sigma_b}{\partial \zeta} = kJ_b + \cdots \quad . \tag{77}$$

In nitrogen, $k \simeq 5 \times 10^{-4}$ cm/statcoulomb.

Even if condition (76a) is satisfied, the tracking force at ζ_p still falls with increasing rise time because the beam current at ζ_p falls. For example, for a pencil beam with constant $\dot{I}_b$,

$$I(a_c, \zeta_p) \leq I_b(\zeta_p) \leq (\dot{I}_b\, a_b/2k)^{1/2}. \tag{78}$$

The decrease in the tracking force is partially offset, however, by an increase in the tracking duration. Moreover, a short beam rise time (i.e., large $\dot{I}_b$) can degrade tracking by initiating avalanching in the inductively generated axial field E_z. On-axis avalanching causes σ_b to rise rapidly so that the pinch point moves forward and $I_b(\zeta_p)$ and the tracking duration are reduced. Optimal beam rise time for maximizing the tracking force at the pinch point is thus expected to occur when the on-axis field $E_z(0, \zeta_p) \simeq E_b$ where E_b is the gas breakdown field strength.

A second influence on tracking is a dipole chemistry effect arising from field dependence in the plasma-electron mobility μ. Hubbard, et al.[16] first discovered this effect in hose studies. A usually adequate expression for the conductivity is

$$\sigma = en_e\mu \tag{79}$$

where n_e is the plasma-electron density. The mobility is defined by

$$\mu = v_d/E \tag{80}$$

where $v_d(E)$ is the plasma-electron drift velocity. Straightforward linearization of the plasma current density, $J_p = \sigma E = en_e v_d$, reveals that the dipole equations (23) and (31) are more accurately represented by

$$\frac{\partial}{\partial r}\frac{1}{r}\frac{\partial}{\partial r} rA_1 = \frac{4\pi}{c}\left[y\frac{\partial}{\partial r}\left(J_b - \sigma_b\frac{\partial A_o}{\partial \zeta}\right) + y\,\sigma_{b1}\frac{\partial}{\partial r}\left(\frac{\partial A_o}{\partial \zeta}\right) + \left(\sigma_{b1} + \sigma_{c1}\right)\frac{\partial A_1}{\partial \zeta}\right] \tag{81}$$

and

$$F_m = \frac{2\pi e\beta}{c}\int_o^\infty dr\left[\hat{I}_b\sigma_{c1}\frac{\partial A_1}{\partial \zeta} - y\frac{\partial \hat{I}_b}{\partial r}\sigma_c\frac{\partial A_o}{\partial \zeta} + \hat{I}_b\sigma_{b1}\frac{\partial A_{1b}}{\partial \zeta}\right], \tag{82}$$

respectively, where the effective "dipole" conductivities are defined by

$$\sigma_{b1} \equiv en_{eb}\mu_d \tag{83}$$

and

$$\sigma_{c1} \equiv en_{ec}\mu_d. \tag{84}$$

Here n_{ec} is the plasma-electron density in the channel, n_{eb} is the plasma-electron density generated symmetrically about and by the beam, and μ_d is the differential mobility given by

$$\mu_d \equiv \frac{\partial v_d}{\partial E} = \left[1 - \frac{\partial \ln(\nu_m)}{\partial \ln(E)}\right]\mu \tag{85}$$

where $\nu_m = eE/m_e v_d$ is an average momentum-transfer collision frequency for the plasma electrons. Not included in these equations are azimuthal asymmetries in n_{eb} caused by avalanching as discussed in the previous section.

The principal change introduced by Eqs. (81) and (82) is that the dipole decay times τ_{c1} and τ_{b1} are determined not by the conductivities σ_c and σ_b but by the effective conductivities σ_{c1} and σ_{b1}. If the collision frequency ν_m increases with field E, as is typical of most weakly ionized gases, the dipole decay times are reduced. The reduction is modest, however, in gases such as nitrogen where $0.5 \lesssim \mu_d/\mu < 1$. Increasing the channel ionization by a factor of two or so is thus often sufficient to insure that condition (15) for τ_{c1} remains satisfied. In unusual[17] or highly ionized gases, μ_d can exceed μ and the dipole decay times are increased. In some gases, μ_d can be negative but the plasma currents are then inherently unstable. In all cases the tracking force never exceeds the value predicted by Eq. (9).

A third effect on tracking is channel fill-in. For some applications, channel fill-in cannot be avoided, and hence a truly hollow channel configuration cannot be maintained. Hollow channels produced by laser preionization, for example, suffer from laser refraction and diffraction which cause the laser beam to optically distort.

The effect of channel fill-in on tracking can be assessed by adding a constant floor conductivity, σ_f, for $r \leq a_c$. If the fill-in conductivity is low ($4\pi\sigma_f a_c/c \lesssim 1$ and $\sigma_f \ll \sigma_{co}$), channel tracking is probably improved because σ_f weakens or eliminates deleterious electrostatic effects. If σ_f is large, however, it produces an overlap detracking force given according to Eq. (31) by

$$F_f = \frac{2\pi e\beta}{c} y\, \sigma_f \bar{E}_{zo} \tag{86}$$

where

$$\bar{E}_{zo} = -\int_o^{a_c} dr\, \frac{\partial \hat{I}_b}{\partial r} \frac{\partial A_o}{\partial \zeta} \tag{87}$$

is an average axial electric field. Because the monopole field, $E_{zo} = -\partial A_o/\partial\zeta$, usually varies slowly with r, the average field satisfies

$$\bar{E}_{zo} \simeq [I(a_c,\zeta) - I_b(\zeta)]/[\pi a_b^2\sigma_b + \pi a_c^2\sigma_f]. \tag{88}$$

If we define the peak channel tracking force by

$$F_t = 2e\beta y I(a_c,\zeta)/a_c c^2, \tag{89}$$

we find that

$$\frac{F_f}{F_t} \simeq -\left(\frac{I_b(\zeta) - I(a_c,\zeta)}{I(a_c,\zeta)}\right)\left(\frac{a_c^2\sigma_f}{a_c^2\sigma_f + a_b^2\sigma_b}\right). \tag{90}$$

This equation indicates that channel fill-in does not appreciably degrade tracking unless it causes the net current inside the channel to fall below

$$I(a_c,\zeta) \lesssim I_b(\zeta)/2. \tag{91}$$

In that case, the net force can become detracking and eject the beam from the channel.

At beam injection, condition (91) is satisfied and the net channel force is detracking, provided $4\pi\sigma_f a_c/c > 1$. The plasma currents in σ_f that cause detracking then relax while the net current $I(a_c,\zeta)$ grows. For $\sigma_b \to 0$, the characteristic relaxation time for the detracking force to decay and $I(a_c\zeta)$ to grow is given by

$$\tau_f = \pi a_c^2 \sigma_f / 2c^2. \tag{92}$$

As $I(a_c, \zeta)$ grows, the tracking force from dipole currents in σ_c develops. The development of this tracking force is hampered, however, by its relaxation on a characteristic time τ_{c1}. Only if

$$\tau_{c1} > \tau_f \tag{93}$$

can the tracking force fully develop and overcome the detracking force caused by plasma currents in σ_f. According to Eqs. (62) and (92), a broad hollow channel of conductivity σ_{co} can therefore produce strong tracking only if the fill-in conductivity satisfies

$$\sigma_f < \sigma_{co}/2. \tag{94}$$

Conversely, if the fill-in conductivity exceeds fifty percent of the off-axis peak conductivity, detracking is likely. Hubbard and Slinker[13] have performed numerical simulations that confirm this prediction.

A fourth effect that can degrade tracking is azimuthal nonuniformity in the channel. Nonuniformity caused by laser hot spots, preferential avalanching, or other means should not be too disruptive provided the nonuniformity is mild. The principal effect is to displace the effective channel center and to produce detracking in the beam body, much as occurs in the magnetic cage. An example of strong nonuniformity is a three-conductor or four-conductor cage with one conductor missing. In that case, the absence of conductivity over a broad region would lead to violent ejection of the beam.

A dynamical effect that invariably degrades tracking is beam expansion. Gas scattering, ohmic losses, and finite beam emittance all cause the beam head to expand and flare radially outward as it advances. This flaring pushes the pinch point ζ_p backward so that the beam head continually erodes.[18,19] Because the channel tracking force is of finite magnitude and extent, any given beam slice experiences a positive tracking force for only a finite time before erosion sweeps past. If the duration is too short to allow the beam to respond, tracking is curtailed. The curtailment is small only if the erosion rate satisfies

$$\frac{d\zeta_p}{dz} < \frac{\Delta\zeta_t}{z_t} . \tag{95}$$

Here $\Delta\zeta_t$ characterizes the extent of the tracking region, and

$$z_t = \frac{\pi}{2} (\gamma mc^2)^{\frac{1}{2}} [y/F_t(y)]^{\frac{1}{2}} \tag{96}$$

characterizes the axial distance required for the tracking force F_t to deflect the beam. For hollow channels with $\Delta\zeta_t \simeq c\tau_{c1}$, erosion can typically be neglected only if

$$c\tau_{c1} > \frac{\pi a_c}{2\beta} \left[\frac{I_A}{2I(a_c,\zeta_p)}\right]^{\frac{1}{2}} \frac{d\zeta_p}{dz} \tag{97}$$

where $I_A = \beta\gamma mc^3/e$ is the Alfven current. Erosion is usually most severe for low-energy beams and often seriously threatens channel tracking.

A related problem is the rise in the beam radius a_{bp} at the pinch point as the beam nears the end of its range. Unless the channel radius a_c increases with propagation distance z, a_{bp} will eventually exceed a_c. The beam is then likely to be ejected from the channel or suffer rapid erosion.

Loss of the beam is inevitable. Such loss is generally of little consequence, however, because the loss occurs only after the beam has lost most of its energy and has begun to rapidly expand.

6. Numerical Simulations

Preliminary numerical simulations using the DYNASTY field solver[20] have partially confirmed the preceding analytical predictions. Typical results for the net tracking force are presented in Fig. 3. In these simulations the beam was displaced by 0.05 cm from the channel center with a beam current density given by

$$J_b(r,\zeta) = (I_{bo}/\pi a_b^2)\exp(-r^2/a_b^2)\tanh(\zeta/\zeta_r). \qquad (98)$$

In all runs avalanching was turned off, to aid comparison with theory, and the beam parameters were: peak current I_{bo} = 10 kA, radius a_b = 0.5 cm, rise length ζ_r = 15 cm, and direct-production coefficient k = 8.8 x 10^{-4} cm/statcoulomb.

In curves a and b of Fig. 3, the preexisting conductivity for the annular channels was given by

$$\sigma_c(r) = \sigma_{co}\exp[-4(r-r_c)^2/\delta r_c^2] \qquad (99)$$

with $\delta r_c = r_c$ = 1 cm. The use of steeper profiles for σ_c led to numerical difficulty. Despite the presence of both substantial channel fill-in and substantial beam-channel overlap, the tracking force was large. In curve a where $4\pi\sigma_{co}a_b/c$ = 5 (with $R_c \simeq 6$ Ω/cm and $c\tau_{c1} \simeq 2$ cm), a peak tracking force of 160 Gauss per cm of beam displacement was reached at ζ = 5 cm. Detracking occurred beyond ζ = 18 cm, but this should be offset by strong body-head coupling. Indeed, channel fill-in caused the pinch

point $\zeta_p \to 0$ in this example. Raising the channel conductivity to $4\pi\sigma_{co}a_b/c = 50$ (with $R_c \simeq 0.6$ Ω/cm and $c\tau_{c1} \simeq 20$ cm) caused the tracking force in curve b to continue rising until it peaked at 575 Gauss per cm at $\zeta = 17.5$ cm.

Curves c and d were derived for a magnetic cage consisting of four solid channels, each displaced symmetrically 1 cm from the cage axis and each with a Gaussian radius of 0.5 cm. The net cage resistance in curve c was $R_c \simeq 6$ Ω/cm while in curve d, $R_c \simeq 0.6$ Ω/cm. Comparison of curves a and c and curves b and d demonstrates that the four-conductor cage degraded the tracking force produced by an equivalent smooth annulus by $\lesssim 20\%$.

In curve e, a low channel conductivity of $4\pi\sigma_{co}a_b/c = 1$ was used, spread over a broad annulus from $r = 0.5$ to 5 cm. The tracking force was reduced but still large and peaked at 36 Gauss/cm. The tracking force persisted for a surprisingly long time. Whether this persistence is an artifact of the code or accurately represents the diffusive decay of the tracking force remains unclear.

7. Summary

The preceding analysis and simulations have shown that hollow channels of even modest conductivity can produce strong tracking forces on relativistic electron beams propagating inside. Such channels have the added advantage of improving stability in the beam head. The combined traits of strong tracking and improved beam stability make hollow channels particularly attractive for both long-range and short-range guidance of charged particle beams.

The principal requirements for successful hollow-channel tracking are high conductivity and conductance in a channel that lies outside the beam. Dipole chemistry effects, slow beam rise, and moderate channel fill-in or nonuniformity may weaken the tracking force but rarely eliminate it. The principal practical obstacles are creating the channel and finding a stable, slowly eroding mode of beam propagation.

Although preliminary numerical simulations have partially confirmed the analysis, further numerical work is required. Static simulations are needed to assess the impact of avalanching on rarefied or weakly preionized channels, and to study the effects of dipole chemistry, beam rise, and channel fill-in and nonuniformity. Dynamical simulations, such as those begun by Hubbard and Slinker,[13] are needed to study beam stability, beam erosion, loss of beam particles that lie outside the annulus, and the behavior of the beam once the pinch point expands outside the channel.

We mention in closing that hollow-channel tracking has been successfully demonstrated in the laboratory by Leifeste, et al.[2] and by Raleigh and Fernsler.[14] Leifeste, et al. used a hollow Nd:YAG laser to preionize an annular channel in nitrogen doped with diethylanaline.

Successful guidance and beam transport were achieved at a gas pressure of 1 Torr with only moderate beam hose. More recently, Raleigh demonstrated beam guidance and partial stabilization at pressures up to 40 Torr in air using a cage constructed of four resistive rods.

Acknowledgements

The authors thank Dr. Richard Hubbard and Dr. Steven Slinker for sharing their numerical results on hollow-channel tracking and stabilization. The comments, suggestions, and encouragement offered by Dr. Martin Lampe are gratefully acknowledged as well. This work was supported by the Defense Advanced Research Projects Agency under ARPA Order No. 4395, Amendment No. 63, and monitored by the Naval Surface Weapons Center.

References

1. R. F. Hubbard, R. F. Fernsler, S. P. Slinker, A. W. Ali, M. Lampe, G. Joyce and J. M. Picone, "Stability of Relativistic Electron Beams in Density Channels I", 5th International Conference on High-Power Particle Beams, San Francisco, CA (Sept., 1983).

2. G. T. Leifeste, C. A. Frost, R. B. Miller, C. Ekdahl and C. Crist, Bull. Am. Phys. Soc. 29, 1292 (1984).

3. H. C. Chen and H. S. Uhm, Bull. Am. Phys. Soc. 29, 1275 (1984).

4. P. A. Miller, R. I. Butler, M. Cowan, J. R. Freeman, J. W. Poukey, T. P. Wright and G. Yonas, Phys. Rev. Lett. 39, 92 (1977).

5. J. R. Greig, D. W. Koopman, R. F. Fernsler, R. E. Pechacek, I. M. Vitkovitsky and A. W. Ali, Phys. Rev. Lett. 41, 174 (1978); D. P. Murphy, M. Raleigh, E. Laikin, J. R. Greig and R. E. Pechacek, "Electron Beam Transport through the Atmosphere in Reduced-Density, Current-Carrying Channels", Proceedings of the Ninth International Symposium on Engineering Problems in Fusion Research, Chicago, Illinois, 1981 (IEEE Publication 81CH1715-2 NPS Vol. II, p. 1548).

6. J. Benford and B. Ecker, Phys. Rev. Lett. 26, 1160 (1971).

7. W. E. Martin, G. J. Caporaso, W. M. Fawley, D. Prosnitz and A. G. Cole, Phys. Rev. Lett. 54, 685 (1985).

8. Result (2) is derived by applying the ultrarelativistic frozen approximation (19) and the Lorentz gauge condition to Ampere's law. No further approximations or assumptions are required.

9. E. P. Lee, "Calculation of a Tracking Force", Lawrence Livermore National Laboratory, UCID-19674 (1983) [DE83006669]; R. J. Briggs, private communication.

10. Expression (14) is used for convenience to characterize when magnetic forces begin to overtake electrostatic forces. Here σ_b is the conductivity evaluated along the beam axis. Other authors define the pinch point differently, depending upon the application.

11. E. P. Lee, Phys. Fluids 21, 1327 (1978).

12. M. Lampe, W. Sharp, R. F. Hubbard, E. P. Lee and R. J. Briggs, Phys. Fluids 27, 2921 (1984).

13. R. F. Hubbard and S. P. Slinker, private communication.

14. M. Raleigh and R. F. Fernsler, "Cage Mode Propagation Experiments", NRL Memorandum Report 5784 (1987).

15. D. P. Murphy, M. Raleigh, R. E. Pechacek and J. R. Greig, "Stability of Relativistic Electron Beams in Density Channels II", 5th International Conference on High-Power Particle Beams, San Francisco, CA (Sept., 1983).

16. R. F. Hubbard, S. P. Slinker, M. Lampe, G. Joyce and R. F. Fernsler, Bull. Amer. Phys. Soc. 29, 1197 (1984). See also R. Hubbard, et al., "Beam Propagation Studies at NRL, Vol. 2", NRL Memorandum Report 5412 (1984). ADA148198

17. T. G. Christophorou, S. R. Hunter, J. G. Carter and R. A. Mathis, Appl. Phys. Lett. 41, 147 (1982).

18. E. P. Lee, "Model of Beam Head Erosion", Lawrence Livermore National Laboratory, UDIC-18768 (Aug. 8, 1980).

19. W. M. Sharp and M. Lampe, Phys. Fluids 23, 2383 (1980).

20. B. Hui and M. Lampe, J. Comp. Phys. 55, 328 (1984).

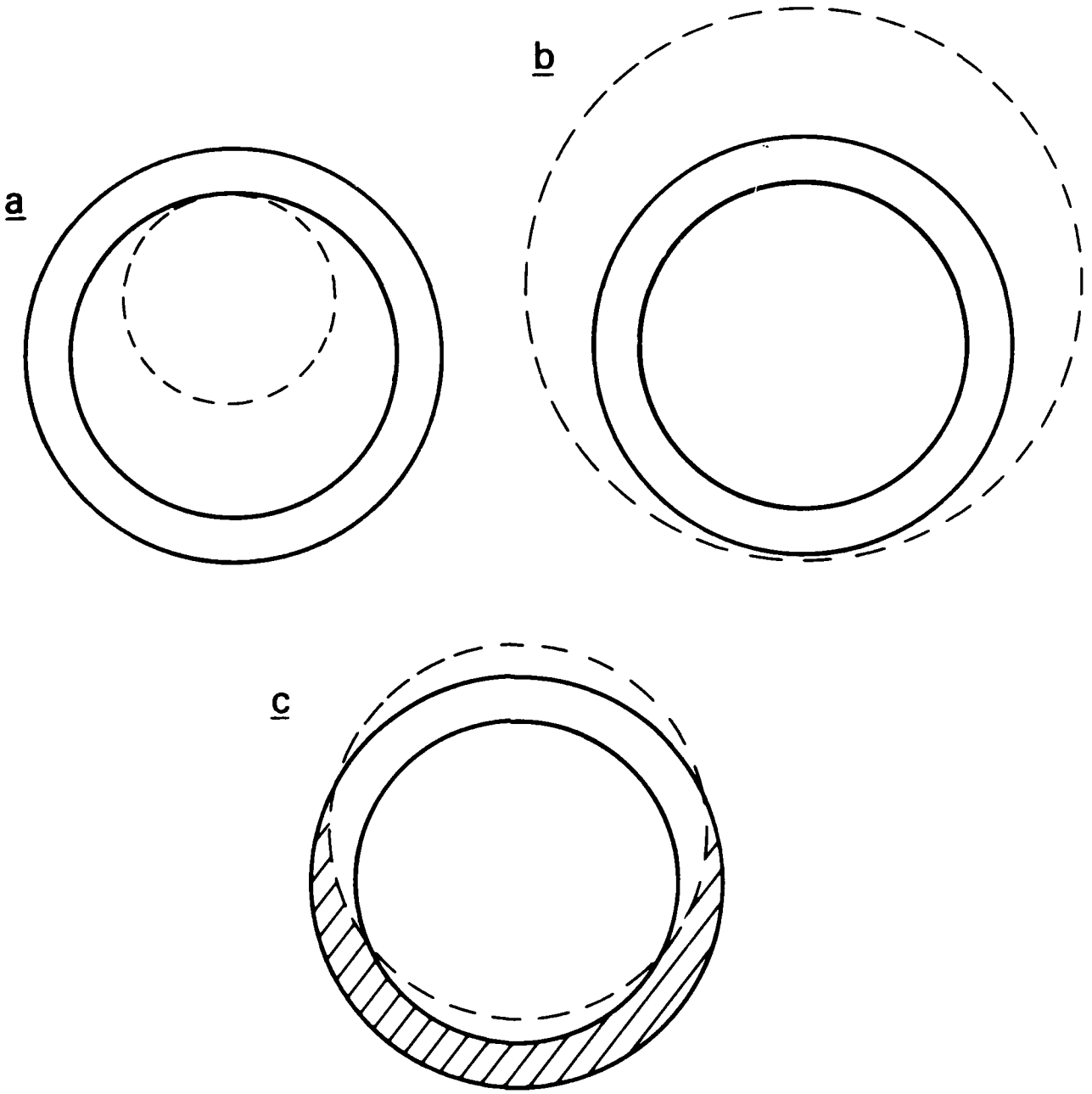

Figure 1. Hollow-Channel Tracking. A displaced electron beam propagates in an annular conducting channel bounded by the heavy concentric circles. A symmetric ring of beam current (dashed circle in a) entirely inside the channel experiences a net tracking force initially and zero force later. A beam ring (b) entirely outside the channel always experiences zero net force. A beam ring (c) intersecting the channel always experiences a net detracking force caused by channel return current flowing outside the ring (shaded area).

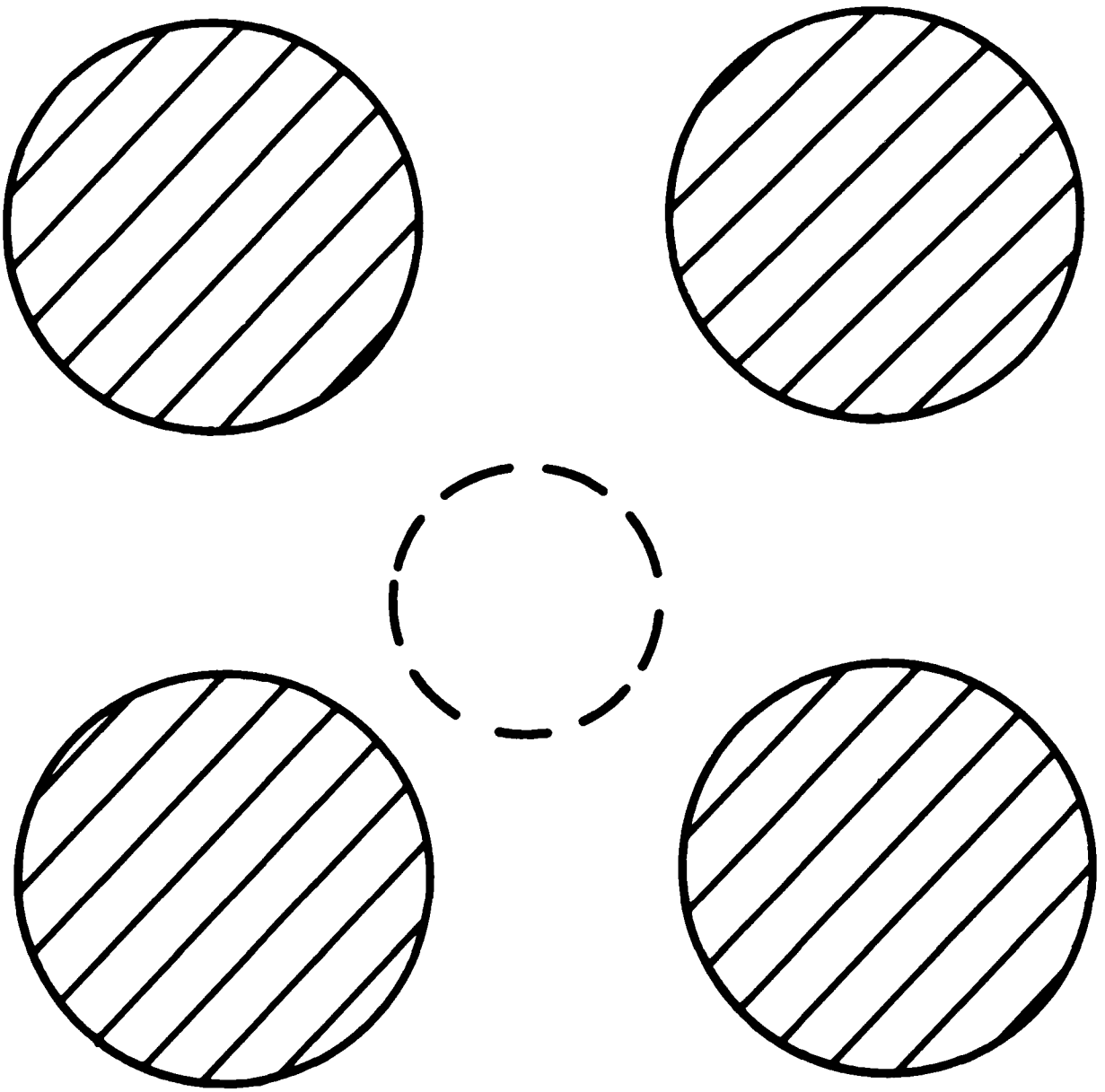

Figure 2. Four-Conductor Magnetic Cage. Four solid conducting (shaded) channels are arranged in a square configuration to guide an electron beam (dashed circle).

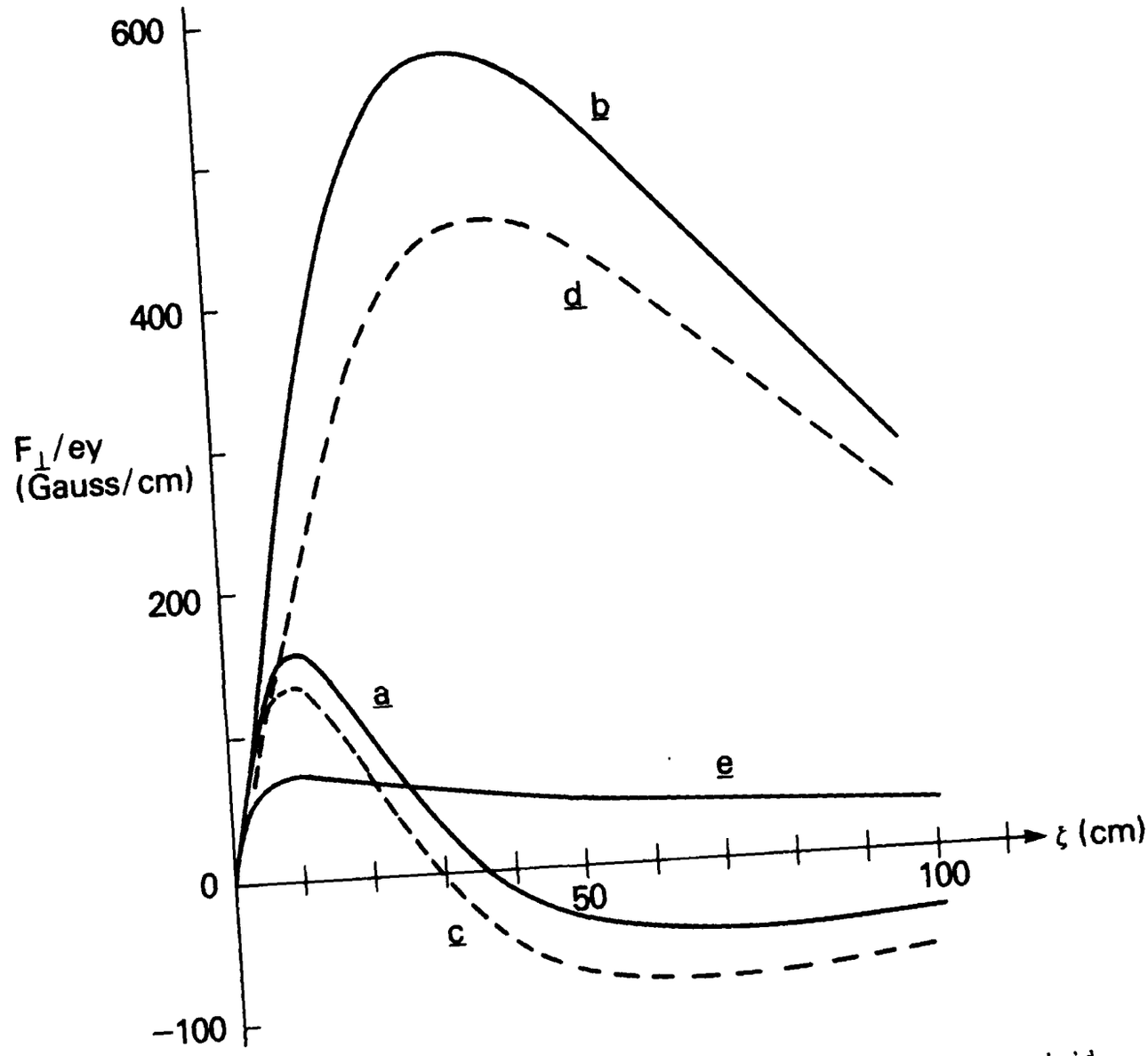

Figure 3. Channel Tracking Force. The net transverse force $F_\perp$ on a rigid-rod beam is plotted versus ζ for: (a) a smooth annular channel with $R_c \simeq 6$ Ω/cm; (b) the same annulus but with $R_c \simeq 0.6$ Ω/cm; (c) a four-conductor cage with $R_c \simeq 6$ Ω/cm; (d) the same cage with $R_c \simeq 0.6$ Ω/cm; and (e) a smooth annulus with $4\pi\sigma_c a_b/c = 1$ between r = 0.5 and 5 cm.

Distribution List

Naval Research Laboratory
4555 Overlook Avenue, S.W.
Washington, D.C. 20375-5000

Attn: Dr. M. Lampe - Code 4792 (2 copies)
Dr. T. Coffey - Code 1001
Dr. J. Boris - Code 4040
Dr. M. Picone - Code 4040
Dr. J. B. Aviles - Code 4665
Dr. M. Haftel - Code 4665
Dr. S. Ossakow - Code 4700 (26 copies)
Dr. A. Ali - Code 4700.1
Dr. M. Friedman - Code 4700.1
Dr. R. Taylor - BRA (4700.1)
Mr. I. M. Vitkovitsky - Code 4701
Dr. S. Gold - Code 4740
Dr. A. Robson - Code 4760
Dr. M. Raleigh - Code 4760
Dr. R. Meger - Code 4763
Dr. D. Murphy - Code 4763
Dr. R. Pechacek - Code 4763
Dr. G. Cooperstein - Code 4770
Dr. D. Colombant - Code 4790
Dr. R. Fernsler - Code 4790 (30 copies)
Dr. I. Haber - Code 4790
Dr. R. F. Hubbard - Code 4790
Dr. G. Joyce - Code 4790
Dr. Y. Lau - Code 4790
Dr. S. P. Slinker - Code 4790
Dr. P. Sprangle - Code 4790
W. Brizzi - Code 4790A
Code 4790 (20 copies)
Library - Code 2628 (20 copies)
D. Wilbanks - Code 2634
Code 1220

Air Force Office of Scientific Research
Physical and Geophysical Sciences
Bolling Air Force Base
Washington, DC 20332
Attn: Major Bruce Smith

Air Force Weapons Laboratory
Kirtland Air Force Base
Albuquerque, NM 87117
Attn: W. Baker (AFWL/NTYP)
D. Dietz (AFWL/NTYP)
Lt Col J. Head

U. S. Army Ballistics Research Laboratory
Aberdeen Proving Ground, Maryland 21005
Attn: Dr. Donald Eccleshall (DRXBR-BM)
Dr. Anand Prakash

Avco Everett Research Laboratory
2385 Revere Beach Pkwy
Everett, Massachusetts 02149
Attn: Dr. R. Patrick
Dr. Dennis Reilly

Ballistic Missile Def. Ad. Tech. Ctr.
P.O. Box 1500
Huntsville, Alabama 35807
Attn: Dr. M. Havie (BMDSATC-1)

Chief of Naval Material
Office of Naval Technology
MAT-0712, Room 503
800 North Quincy Street
Arlington, VA 22217
Attn: Dr. Eli Zimet

Cornell University
369 Upson Hall
Ithaca, NY 14853
Attn: Prof. David Hammer

DASIAC - DETIR
Kaman Tempo
25600 Huntington Avenue, Suite 500
Alexandria, VA 22303
Attn: Mr. F. Wimenitz

Defense Advanced Research Projects Agency
1400 Wilson Blvd.
Arlington, VA 22209
Attn: Dr. Shen Shey
Dr. H. L. Buchanan

Department of Energy
Washington, DC 20545
Attn: Dr. Wilmot Hess (ER20:GTN,
High Energy and Nuclear Physics)
Mr. Gerald J. Peters (G-256)

Directed Technologies, Inc.
226 Potomac School Road
McLean, VA 22101
Attn: Dr. Ira P. Kuhn
Dr. Nancy Chesser

C. S. Draper Laboratories
555 Technology Square
Cambridge, Massachusetts 02139
Attn: Dr. E. Olsson
Dr. L. Matson

Institute for Fusion Studies
University of Texas at Austin
RLM 11.218
Austin, TX 78712
Attn: Prof. Marshall N. Rosenbluth

Intelcom Rad Tech.
P.O. Box 81087
San Diego, California 92138
Attn: Dr. W. Selph

Joint Institute for Laboratory
Astrophysics
National Bureau of Standards and
University of Colorado
Boulder, CO 80309
Attn: Dr. Arthur V. Phelps

Kaman Sciences
1500 Garden of the Gods Road
Colorado Springs, CO 80933
Attn: Dr. John P. Jackson

Lawrence Berkeley Laboratory
University of California
Berkeley, CA 94720
Attn: Dr. Edward P. Lee

Lawrence Livermore National Laboratory
University of California
Livermore, California 94550
Attn: Dr. Richard J. Briggs
Dr. Simon S. Yu
Dr. Frank Chambers
Dr. James W.-K. Mark, L-477
Dr. William Fawley
Dr. William Barletta
Dr. William Sharp
Dr. Daniel S. Prono
Dr. John K. Boyd
Dr. Kenneth W. Struve
Dr. John Clark
Dr. George J. Caporaso
Dr. William E. Martin
Dr. Donald Prosnitz

Lockheed Missiles and Space Co.
3251 Hanover St.
Bldg. 205, Dept 92-20
Palo Alto, CA 94304
Attn: Dr. John Siambis

Los Alamos National Scientific Laboratory
P.O. Box 1663
Los Alamos, NM 87545
Attn: Dr. L. Thode
Dr. M. A. Mostrom, MS-608
Dr. H. Dogliani, MS-5000
Dr. R. Carlson
Ms. Leah Baker, MS-P940
Dr. Carl Ekdahl

Maxwell Laboratories Inc.
8888 Balboa Avenue
San Diego, CA 92123
Attn: Dr. Ken Whitham

McDonnell Douglas Research Laboratories
Dept. 223, Bldg. 33, Level 45
Box 516
St. Louis, MO 63166
Attn: Dr. Evan Rose
Dr. Carl Leader

Mission Research Corporation
EM Systems Applications
1720 Randolph Road, S.E.
Albuquerque, NM 87106
Attn: Dr. Brendan Godfrey
Dr. Thomas Hughes
Dr. Lawrence Wright
Dr. A. B. Newberger

Mission Research Corporation
P. O. Draver 719
Santa Barbara, California 93102
Attn: Dr. C. Longmire
Dr. N. Carron

National Bureau of Standards
Gaithersburg, Maryland 20760
Attn: Dr. Mark Wilson

Naval Surface Weapons Center
White Oak Laboratory
Silver Spring, Maryland 20903-5000
Attn: Dr. R. Cawley
Dr. J. W. Forbes
Dr. B. Hui
Mr. W. M. Hinckley
Mr. N. E. Scofield
Dr. E. C. Whitman
Dr. M. H. Cha
Dr. H. S. Uhm
Dr. R. Fiorito
Dr. K. T. Nguyen
Dr. R. Stark
Dr. R. Chen

Office of Naval Research
800 North Quincy Street
Arlington, VA 22217
Attn: Dr. C. W. Roberson
Dr. M. Moss

Office of Naval Research (2 copies)
Department of the Navy
Code 01231C
Arlington, VA 22217

Office of Under Secretary of Defense
Research and Engineering
Room 3E1034
The Pentagon
Washington, DC 20301
Attn: Mr. John M. Bachkosky

ORI, Inc.
1375 Piccard Drive
Rockville, MD 20850
Attn: Dr. C. M. Huddleston

Physical Dynamics, Inc.
P.O. Box 1883
La Jolla, California 92038
Attn: Dr. K. Brueckner

Physics International, Inc.
2700 Merced Street
San Leandro, CA. 94577
Attn: Dr. E. Goldman

Princeton University
Plasma Physics Laboratory
Princeton, NJ 08540
Attn: Dr. Francis Perkins, Jr.

Pulse Sciences, Inc.
600 McCormack Street
San Leandro, CA 94577
Attn: Dr. Sidney Putnam
Dr. John Bayless

Sandia National Laboratory
Albuquerque, NM 87115
Attn: Dr. Bruce Miller
Dr. Collins Clark
Dr. Barbara Epstein
Dr. John Freeman
Dr. Charles Frost
Dr. Gordon T. Leifeste
Dr. Gerald N. Hays
Dr. James Chang
Dr. Michael G. Mazerakis
Dr. John Wagner
Dr. Ron Lipinski

Science Applications Intl. Corp.
P. O. Box 2351
La Jolla, CA 92038
Attn: Dr. Rang Tsang

Science Applications Intl. Corp.
5150 El Camino Road
Los Altos, CA 94022
Attn: Dr. R. R. Johnston
Dr. Leon Feinstein
Dr. Douglas Keeley

Science Applications Intl. Corp.
1710 Goodridge Drive
McLean, VA 22102
Attn: Mr. W. Chadsey
Dr. A Drobot
Dr. K. Papadopoulos

Commander
Space & Naval Warfare Systems Command
PMW-145
Washington, DC 20363-5100
Attn: CAPT J. D. Fontana
CDR W. Bassett

SRI International
PS0-15
Molecular Physics Laboratory
333 Ravenswood Avenue
Menlo Park, CA 94025
Attn: Dr. Donald Eckstrom

Strategic Defense Initiative Org.
1717 H Street, N. W.
Washington, DC 20009
Attn: Lt Col R. L. Gullickson
Dr. J. Ionson
Dr. D. Duston

Strategic Defense Initiative Office
Directed Energy Weapons Office, The
Pentagon
Office of the Secretary of Defense
Washington, DC 20301-7100
Attn: Dr. C. F. Sharn (OP0987B)

Titan Systems, Inc.
9191 Towne Centre Dr.-Suite 500
San Diego, CA 92122
Attn: Dr. R. M. Dowe

University of California
Physics Department
Irvine, CA 92664
Attn: Dr. Gregory Benford

University of Maryland
Physics Department
College Park, MD 20742
Attn: Dr. Y. C. Lee
Dr. C. Grebogi

University of Michigan
Dept. of Nuclear Engineering
Ann Arbor, MI 48109
Attn: Prof. Terry Kammash
Prof. R. Gilgenbach

Director of Research
U.S. Naval Academy
Annapolis, MD 21402 (2 copies)